This manuscript was accepted by Phys. Fluids. Click here to see the version of record.

Effective mean free path and viscosity of confined gases

Jianfei Xie,[1, a)] Matthew K. Borg,[2, b)] Livio Gibelli,[2, c)] Oliver Henrich,[3, d)] Duncan A. Lockerby,[4, e)] and Jason M. Reese[2, f)]

[1)]*School of Engineering, University of Derby, Derby, DE22 1GB, UK*

[2)]*School of Engineering, University of Edinburgh, Edinburgh, EH9 3FB, UK*

[3)]*Department of Physics, University of Strathclyde, Glasgow, G4 0NG, UK*

[4)]*School of Engineering, University of Warwick, Coventry, CV4 7AL, UK*

(Dated: 15 June 2019)

The molecular mean free path (MFP) of gases in confined geometries is numerically evaluated by means of the direct simulation Monte Carlo (DSMC) method and molecular dynamics (MD) simulations. Our results show that if calculations take into account not only intermolecular interactions between gas molecules, but also collisions between gas molecules and wall atoms, then a space-dependent MFP is obtained. The latter, in turn, permits one to define an effective viscosity of confined gases that also varies spatially. Both the gas MFP and viscosity variation in surface-confined systems have been questioned in the past. In this work we demonstrate that this effective viscosity derived from our MFP calculations is consistent with those deduced from the linear-response relationship between the shear stress and strain rate using independent non-equilibrium Couette-style simulations, as well as the equilibrium Green-Kubo predictions.

Keywords: rarefied gas; mean free path; near-wall viscosity; direct simulation Monte Carlo; molecular dynamics

[a)]Electronic mail: j.xie@derby.ac.uk

[b)]Electronic mail: matthew.borg@ed.ac.uk; *corresponding author*

[c)]Electronic mail: livio.gibelli@ed.ac.uk.

[d)]Electronic mail: oliver.henrich@strath.ac.uk

[e)]Electronic mail: duncan.lockerby@warwick.ac.uk

[f)]Prof. Jason M. Reese is deceased (March 2019)

This manuscript was accepted by Phys. Fluids. Click here to see the version of record.

I. INTRODUCTION

Rarefied gas flows are of ongoing interest, because of their fundamental nature and many applications in different fields including aerodynamics and heat transfer[29,44], micro/nano-electro-mechanical systems (MEMS/NEMS)[12], and shale gas recovery[14,41]. The traditional dimensionless measure of the degree of rarefaction is the Knudsen number (Kn), defined as the ratio of the molecular mean free path (MFP) to the characteristic dimension of the gas flow.

Rarefaction effects cause gas flows to deviate from continuum fluid behaviour when $\mathrm{Kn} \gtrsim 10^{-3}$. More specifically, for moderate Knudsen numbers in the slip flow regime ($10^{-3} \lesssim \mathrm{Kn} \lesssim 10^{-1}$), these effects are confined to thin layers close to the bounding surfaces, which are referred to as Knudsen layers. These layers may be accounted for in the conventional Navier-Stokes description with slip/jump boundary conditions for the velocity and temperature[12]. In the transition flow regime ($0.1 \lesssim \mathrm{Kn} \lesssim 1$), rarefaction effects become appreciable in the whole domain, and, in principle, the accurate description of a gas flow requires the solution of the Boltzmann equation or simplified kinetic model equations[12]. Thermodynamic non-equilibrium gas flows are met in different physical situations ranging from low pressure conditions in the upper regions of planetary atmospheres (i.e. low-density gas flows in near-vacuum environments) to high pressure conditions in very small channels (i.e. dense gas flows in micro/nano confinements).

Solving gas kinetic equations, either by the stochastic direct simulation Monte Carlo (DSMC) technique[8], or by deterministic methods[4,16], such as molecular dynamics (MD), is computationally demanding, especially for flows that are three-dimensional and/or involve both continuum and rarefied regions[35]. Therefore, much effort has been done over the years to extend the continuum fluid dynamics description to the transition regime. A first approach to incorporating rarefaction effects into a continuum description relies on the higher-order continuum equations that are derived from the kinetic equations via the Chapman-Enskog series solution technique, the Grad moment method, or a combination of these two[37]. A second and simpler approach consists in using an *effective viscosity* with the original strain-rate in the linear constitutive relationship of the Navier-Stokes equations, i.e.

$$\mu_{\mathrm{eff}}(z) = \frac{1}{\Psi(z)}\mu_0, \tag{1}$$

where μ_0 is the nominal viscosity of the gas, and $\Psi(z)$ is an expression of the high-order non-linear correction terms, which depends on the normal distance z to the nearest solid wall[22,24–27]. The effective gas viscosity simplifies to the nominal viscosity in the gas flow regions where rarefaction

effects can be disregarded, i.e., $\Psi(z) \to 1$ as $z \to \infty$ in Eq. (1).

The simplest way to define an effective viscosity is to use the direct proportionality between viscosity and the molecular mean free path (MFP) as predicted by elementary kinetic theory arguments in *equilibrium* conditions[13,23]. Accordingly, this produces a high-order non-linear correction term as follows:

$$\Psi(z) = \frac{\lambda_0}{\lambda_{\text{eff}}(z)}, \tag{2}$$

where λ_0 is the nominal MFP in the space-homogeneous conditions, and λ_{eff} is the *effective* MFP of gas molecules in confined geometries. The nominal MFP for hard-sphere molecules is rigorously defined as:

$$\lambda_{0,h} = \frac{m}{\sqrt{2}\pi d^2 \rho}, \tag{3}$$

while for molecules interacting through long-range potentials, it can be qualitatively expressed as[12]:

$$\lambda_{0,v} = \frac{\mu_0}{\rho}\sqrt{\frac{\pi m}{2k_B T}}. \tag{4}$$

In Eqs. (3) and (4), ρ is the gas density, m is the molecular mass, d is the molecular diameter, T is the temperature of the gas, and k_B is the Boltzmann constant.

Stops[36] first derived a space-dependent expression for λ_{eff} of gas molecules leaving a wall, distributed according to the diffusive Lambert's cosine law of reflection. Several decades later, Guo et al.[20] extended the Stops' model to propose the MFP of confined gases as:

$$\frac{\lambda_{\text{eff},G}(z)}{\lambda_0} = 1 - \frac{1}{2}\left[z^2 E_1(z) + (1-z)e^{-z}\right], \tag{5}$$

where $E_1(z)$ is the exponential integral function, i.e. $E_1(z) = \int_z^\infty e^{-z}/z\,\mathrm{d}z$. More recently, Abramov[1,2] has introduced a new expression for the MFP of gases in confined geometries by replacing the cosine law with the equilibrium Maxwellian to give:

$$\frac{\lambda_{\text{eff},A}(z)}{\lambda_0} = 1 - \frac{1}{2}\left[e^{-z} - yE_1(z)\right]. \tag{6}$$

Beside theoretical research in this area, there have been a number of recent studies in which molecular dynamics (MD) simulations have been used to directly evaluate the MFP in a gas by averaging the recorded individual free paths[5,7,17,31,39]. However, there is still debate about the behaviour of the effective MFP in confined geometries, and whether this is physical or not. Some studies take into account the collisions between the freely moving gas molecules and wall atoms, as these are momentum-changing events, and show that the MFP varies near surfaces[5,17,31,39].

This manuscript was accepted by Phys. Fluids. Click here to see the version of record.

Others[7] have argued that the collisions between the freely moving gas molecules and solid wall atoms (or gas molecules adsorbed on the walls) should be disregarded when evaluating the individual free paths. The latter study shows that the MFP should not vary spatially and conclude that the effective viscosity provided by Eq. (1) is questionable[7].

The main aim of the present paper is to resolve disputes in the literature about the spatial variation of the MFP for gases in confined geometries, such as in flows through micro/nanochannels. For this purpose, the MFP is computed numerically now by means of both DSMC and MD on the basis of its definition, namely by averaging the distance travelled by molecules between two consecutive collisions. Our aim is also to demonstrate using different techniques for measurements of viscosity that there *is* a variation in viscosity near a surface, thereby validating Eq. (1).

It is the first time that DSMC has been used for this kind of investigation until now. The DSMC technique offers a number of advantages compared to MD simulations, such as the computational efficiency and the possibility to more easily assess the theoretical predictions proposed in the literature[2,20]. On the other hand, MD remains the key simulation tool in that, in principle, it enables the study of more complex and realistic fluid flows[14,43], including the important gas-surface interactions.

The rest of the paper is organised as follows. In Section II, we briefly present the DSMC and MD approaches, and we discuss the procedure for the direct determination of the MFP. In Section III, we first investigate how the MFP of gas molecules is modified when their dynamics are constrained by a confining geometry and we assess the accuracy of the theoretical predictions proposed so far, i.e. Eqs. (5) and (6) (Subsection III A). We then measure viscosity using independent methods and compare our results with Eq. (1) in Subsection III B. Conclusions and future work are then drawn in Section IV.

II. EVALUATION OF MOLECULAR MEAN FREE PATHS

A. Direct simulation Monte Carlo

The DSMC technique was initially introduced for gas simulations based on physical arguments[8], but it has been proved to converge, in a suitable limit, to the solution of the Boltzmann equation[40]. The basic idea of DSMC consists in representing the velocity distribution function of the gas molecules by a number of computational particles. Particle motion and interactions

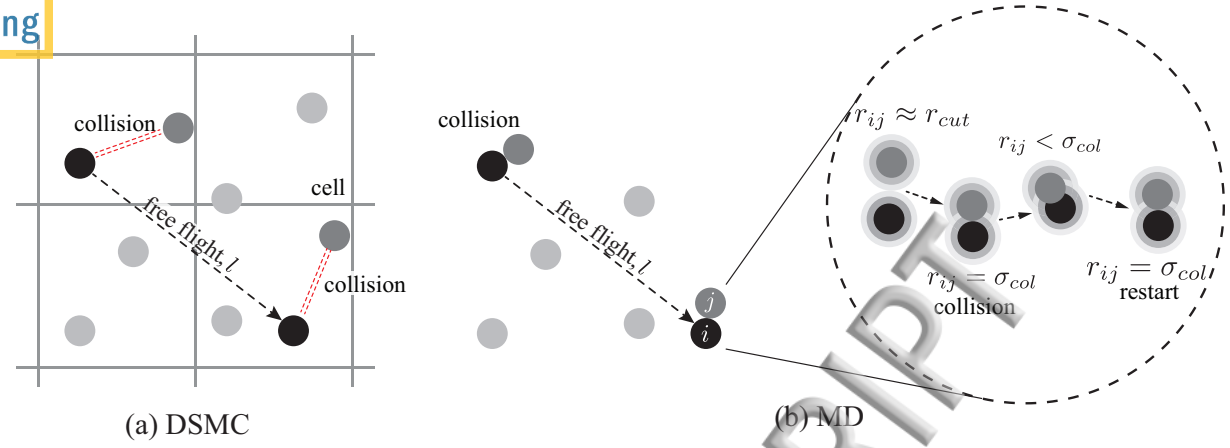

(a) DSMC (b) MD

FIG. 1: Schematic of the calculation of individual free paths in our (a) direct simulation Monte Carlo and (b) Molecular Dynamics simulations.

are decoupled over a time step Δt, which is smaller than the average collision time. The space domain to be simulated is divided into a mesh of cells whose size Δz is less than the MFP. These cells are used to collect together particles that may collide according to stochastic rules derived from the Boltzmann equation. The cells employed for simulating interactions are also used for the sampling of macroscopic properties, which are obtained through weighted averages of the particle properties.

In the present work, particles' collisions are evaluated based on the hard sphere molecular model, which provides a reliable description of isothermal gas flows of argon-like molecules. The particles' free paths are evaluated by tagging particles and keeping track of their free flight distance by an appropriate counter that measures the distance incremented by a particle in each time step, as shown in Fig. 1(a). The free path is therefore a sum over all displacements between two successive collisions:

$$l_i(z) = \sum_{j=1}^{n} v_{i,j}\, \Delta t, \tag{7}$$

where $v_{i,j}$ is the speed of the ith particle at time t_j, n is the number of time steps between two successive collisions, z is the coordinate of the bin where the particle collided, and Δt is the numerical time step. Note that if external force fields are absent, such as in the case of DSMC, the particle's velocity between two consecutive collisions is constant and, therefore, it can be taken out of the sum. When a particle collides, the free path is terminated, and the counter is set to zero whether the collision occurred with a wall or with another particle. As particle-particle collisions occur in a DSMC cell, the free path is also collected and assigned to the same cell for further

post-processing.

The mean free path is then easily obtained by averaging over particles:

$$\lambda(z) = \frac{\sum_{i=1}^{N} l_i(z)}{N(z)}, \tag{8}$$

where $N(z)$ is the total number of particles that have terminated their free path in the bin of coordinate z. Our numerical experiments have shown that the MFP is discontinuous if the free flights of the molecules hitting the walls are attributed to the cells closest to them. The continuity of the MFP is recovered by setting to zero the counter of molecules which suffer a collision with walls, but disregarding their free flight contribution.

The DSMC simulations we report below have been obtained with $\Delta z = 10^{-2}\lambda_0$ and $\Delta t = 2 \times 10^{-3} t_0$, where $t_0 = \lambda_0/(k_B T_0/m)$, and λ_0 and T_0 are the nominal mean free path and a reference temperature, respectively. Computational particles are initially distributed according to a Maxwellian at the temperature T_0 and their average number per cell during simulations is about 10^2. The evolution of the system is simulated for $10^3 t_0$. As an input parameter for the boundary condition, both fully diffusive wall, i.e. the tangential momentum accommodation coefficient (TMAC) $\alpha = 1.0$, and a mixture of partially diffusive and partially specular walls (i.e. $\alpha < 1.0$) have been used in our DSMC simulations: four values of the TMAC (i.e. $\alpha = 0.2$, 0.4, 0.6, 0.8 and 1.0) are tested. Our results show that the influence of the TMAC on the calculations of MFP is negligible. For the sake of simplicity, the fully diffusive wall is adopted in all our DSMC simulations below.

B. Molecular dynamics

In MD simulations, the molecules move according to Newton's second law, and the intermolecular interactions are modelled through a prescribed interatomic potential. In the present study, monatomic argon (Ar) gas is used and it is assumed that molecules interact through the Lennard-Jones (LJ) potential:

$$U^{LJ}(r_{ij}) = \begin{cases} 4\varepsilon\left[\left(\dfrac{\sigma}{r_{ij}}\right)^{12} - \left(\dfrac{\sigma}{r_{ij}}\right)^{6}\right], & r_{ij} \le r_c, \\ 0, & r_{ij} > r_c, \end{cases} \tag{9}$$

TABLE I: Physical parameters and their values in our MD simulations. Subscripts Ar and Pt refer to argon and platinum atoms, respectively, and k_B is the Boltzmann constant.

Parameter	Symbol	Value
Length scale	σ_{Ar}	3.405×10^{-10} [m]
	σ_{Ar-Pt}	3.085×10^{-10} [m]
Energy scale	ε_{Ar}	1.67×10^{-21} [J]
	ε_{Ar-Pt}	0.894×10^{-21} [J]
Molecule mass	m_{Ar}	6.63×10^{-26} [kg]
	m_{Pt}	3.24×10^{-25} [kg]
Time scale	$\tau = \sigma_{Ar}\sqrt{m_{Ar}/\varepsilon_A}$	2.15×10^{-12} [s]
Temperature	ε_{Ar}/k_B	119.8 [K]

where r_{ij} is the intermolecular distance, ε is the energy parameter, σ is the molecular diameter, and r_c is the cutoff distance.

For the measurement of individual free paths, as shown in Fig. 1(b), a condition is set to judge the occurrence of a collision event between gas molecules: if the distance between two gas molecules is equal to or less than the collision diameter σ_{col}, i.e. $r_{ij} \leq \sigma_{col}$, the two molecules have collided and we stop recording the free paths of the involved molecules. We describe the procedure used to define the collision diameter in our MD simulations, in Appendix A.

As the LJ potential allows any pair of molecules to move closer to each other, even when $r_{ij} < \sigma_{col}$, then the finite time spent during this collision process must be excluded when calculating the individual free paths. Therefore, we restart recording the free paths when the distance between the molecules is again larger than the collision diameter, i.e. when $r_{ij} > \sigma_{col}$. In this procedure, the counter for recording each molecular free path is switched on after the last collision between two molecules and it is not switched off until the next collision. We also count collisions between gas molecules and wall atoms: if the gas molecule approaches a wall and crosses a *virtual* plane that is placed σ_{col} away from and parallel to the wall, we say it has collided with the wall and stop recording its free path. The MFP is computed using the same equations in the DSMC setup, namely Eqs. 7 and (8). Note that, in MD simulations particles' velocities are not constant between

This manuscript was accepted by Phys. Fluids. Click here to see the version of record.

ing consecutive collisions because of the long range nature of the Lennard-Jones potential.

The open source code LAMMPS[32] is used to perform our MD simulations reported below, and a new class has been developed to calculate the individual molecular free paths. The potential is truncated at a cutoff of $r_c = 2.5\sigma_{Ar}$, and the neighbour list method is adopted to reduce the time-consuming calculation of intermolecular interactions[3]. A Nosé-Hoover thermostat is applied to all gas molecules but only in the relaxation part of the simulation, until the system reaches an equilibrium state (i.e. typically the first 1.5×10^6 time steps in our MD simulations); the thermostat is then switched off to remove its effect on the dynamics of the gas molecules while the individual free paths are recorded. We spend about 2×10^6 additional time steps averaging the macroscopic properties and the MFP. Wall atoms are chosen to be platinum (Pt), and the gas-wall (Ar-Pt) interaction is also modelled with the Lennard-Jones potential. The parameters and their values that are used in our MD simulations are listed in Table I. The mixed length and energy scales $\sigma_{Ar-Pt} = 3.085 \times 10^{-10}$ m and $\varepsilon_{Ar-Pt} = 0.894 \times 10^{-21}$ J, respectively, are obtained using the Lorentz-Berthelot mixing rules[3,34].

Platinum atoms form two planes of a face-centred cubic (FCC) lattice, i.e. four layers of solid wall atoms, and are tethered to the lattice site with a harmonic spring which vibrates at the Einstein frequency[10,42]. A velocity rescaling thermostat is applied to all wall molecules at the same temperature as the gas throughout the MD simulations. We keep the number of wall atoms the same in our simulations (i.e. 358,688 platinum atoms in each solid wall) for all Kn. Note that the lattice space between each layer is $1.154\sigma_{Ar}$, so the thickness of each solid wall is $3.462\sigma_{Ar}$, which is about 1.5 times larger than the interatomic potential cutoff distance of $2.5\sigma_{Ar}$ in the MD simulations. This thickness of solid wall guarantees that the influence of the furthest layer of wall atoms on our gas molecular calculations of the free paths is negligible. We also observe in our MD simulations that gas adsorption on the solid surface is negligible. The number of gas molecules in the microchannel is 137,952 for Kn = 0.05; as Kn increases (i.e. the channel height decreases), the number of gas molecules decreases accordingly. The equations of motion are integrated using a velocity Verlet algorithm with a time step of $\Delta t = 2 \times 10^{-3}\tau$, where the characteristic time unit τ is given in Table I. The spatial variation of the MFP is obtained by assigning the individual free paths to small constant-width bins that divide the space in the z-direction[17,31,39]. The bin-independence of MD results has been tested by varying the number of bins from 100 to 2000. It is found that the MFP profiles across the channel do not significantly change beyond 500 bins for Kn = 0.2, 1000 bins for Kn = 0.1, and 2000 bins for Kn = 0.05. These correspond to the same bin width in each

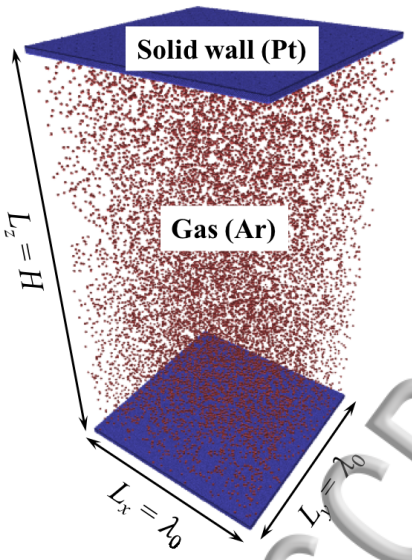

FIG. 2: MD simulation: sample configuration of argon (Ar) gas confined in a microchannel at standard temperature and pressure.

case. The MD results reported below use these numbers of bins.

III. RESULTS AND DISCUSSION

A. Mean free path of confined gases

We consider a gas in equilibrium at standard temperature and pressure confined in a microchannel and evaluate the MFPs using both DSMC and the MD techniques. In the DSMC simulations, the computational domain is one-dimensional (z direction). In the MD simulations, the two solid walls are parallel to the xy plane and periodic boundary conditions are imposed along the x and y directions, as shown in Fig. 2. The distance between the two parallel walls in the z direction is H, and the lengths in both x and y directions are set to λ_0, which is the nominal MFP. We simulate cases with different z-direction distances between the two parallel walls, varying from $20\lambda_0$ to $\lambda_0/2$, where λ_0 is the nominal MFP given by Eq. (3). These correspond to Kn ranging from 0.05 to 2.

As the collisions between gas molecules and wall atoms are momentum-changing events, we have taken these into account when recording the free paths. However, below we also investigate a different free path definition that does not include them.

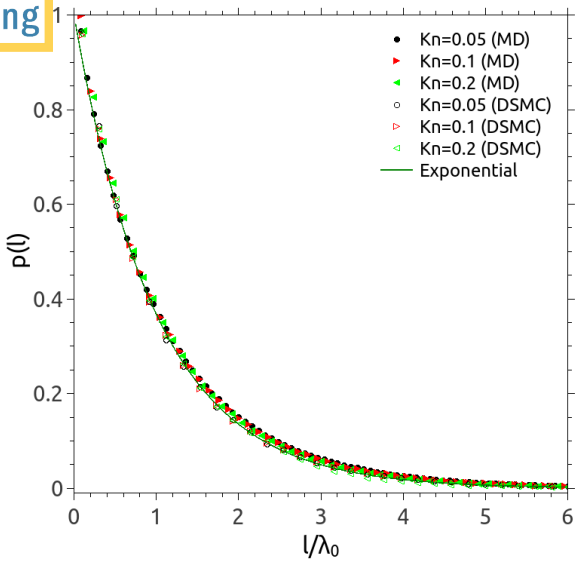

(a) Kn = 0.05, 0.1, 0.2

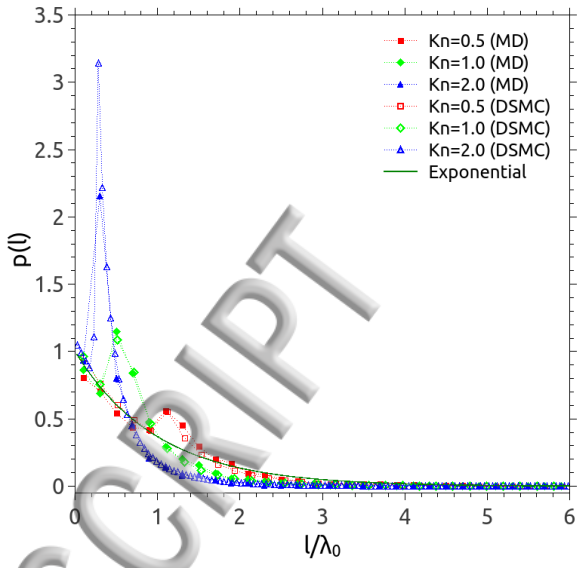

(b) Kn = 0.5, 1, 2

FIG. 3: Probability density distribution of the individual free paths of gas molecules in the middle of channels provided by MD and DSMC simulations for different Knudsen numbers: (a) Kn = 0.05, 0.1, 0.2 and (b) Kn = 0.5, 1, 2.

The influence of a solid wall on the MFP can be first investigated by examining the probability distribution of the individual free paths across the channel. In elementary kinetic theory, the free path distribution of gas molecules is supposed to be exponential in a homogeneous system (i.e. when the gas is not bounded by solid surfaces), which we verify is the case in both our MD and DSMC simulations. However, the free path of gas molecules can be terminated at the wall in confined geometries (i.e. an inhomogeneous case) if gas-wall collisions are counted, which produces a power-law distribution of the free paths[17]. Therefore, to assess the effect of solid walls, we measure the free path distributions of gas molecules in the middle of channels with different heights. Figure 3(a) shows that the free path distributions are still essentially exponential at small Kn (i.e. in the upper slip and early transition regimes). However, as shown in Fig. 3(b), when Kn $\gtrsim$ 0.5, spikes are observed in the distributions of the free paths; these spikes are caused by the presence of the solid walls and move to the smaller free paths as Kn increases. The simulation results of the DSMC and MD are in good agreement.

As can be seen in Fig. 4, the measured MFP varies near the wall, and at the wall is half the nominal value it has in the bulk. It is worth stressing that the small spatial gap between the surface and the MD data for Kn = 0.2 is not physical, but is due to the assignment of the value of a MFP

in a measurement bin to the central point of that bin; this becomes more noticeable at larger Kn. The spatial extent of the near-wall zone becomes greater with increasing Kn. At small Kn, the MD results agree well with the DSMC results and Abramov's theoretical prediction[1], i.e. Eq. (6), while the expression of Guo *et al.*[20], i.e. Eq. (5), somewhat underpredicts the MFP near the walls. Note that To *et al.*[39] obtained a MFP of zero near the wall in their MD simulations for Kn = 0.18 and 0.37, but they only considered molecules outgoing from the walls.

As mentioned earlier, authors from a previous study[7] have argued that the MFP should be defined as the average distance between successive collisions of gas molecules only, and that collisions between gas molecules and wall atoms or gas molecules adsorbed on a wall surface should not be taken into account when evaluating individual free paths. With such a definition, a constant and isotropic MFP would be expected. In order to assess this prediction, we have run MD and DSMC simulations in a microchannel ($H = 20\lambda_0$) and disregarded gas-wall collisions in the evaluation of the MFP. More specifically, while interactions between gas molecules and wall atoms are still part of the dynamics, the individual free paths are not terminated at the walls. Our simulations show that a constant MFP is predicted by both DSMC and MD simulations when the walls are perfectly specular (i.e. $\alpha = 0$), and Fig. 5 shows that a constant MFP is also obtained when fully diffusive (DSMC) and real (MD) walls are used.

We therefore conclude that a space-dependent MFP in confined geometries (i.e. an inhomogeneous case) is simply a consequence of taking into account the gas-wall collisions. This result is not in disagreement with the classical expression in kinetic theory that relies on the assumption of spatially homogeneous conditions. Collisions between the gas and bounding surfaces can be incorporated in the concept of the MFP and, as discussed in the literature[1,2,5,20,39], the resulting spatial variation of the MFP may help in understanding the transport of gases in Knudsen layers near surfaces.

B. Local viscosity of the gas in near-wall regions

If the MFP is constant in micro/nanochannels, i.e. the collision rate is on average constant everywhere, this indicates that the viscosity of the fluid behaves homogeneously too, and the system under a constant shear stress should give a linear velocity profile. We know that this is not true for gases in thermodynamic non-equilibrium, and we believe the hypothesis that there is a constant MFP in these systems is not a practical one either. The reason having an effective

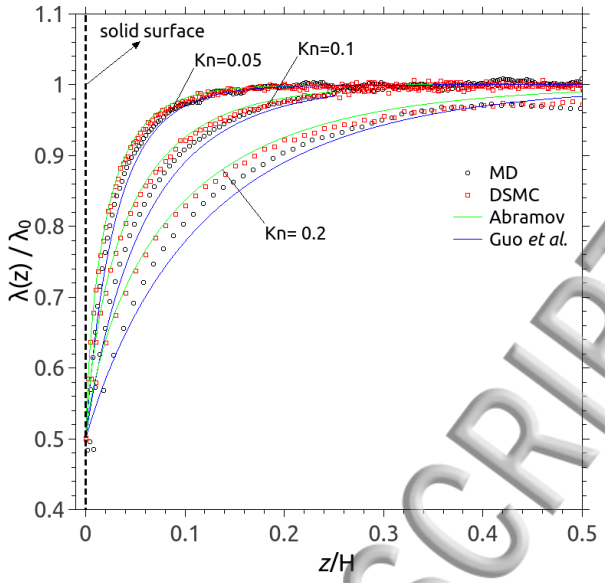

FIG. 4: Spatial variation of the normalised MFP in microchannels using DSMC (open squares) and MD (open circles). The theoretical predictions of Guo *et al.*[20] (blue solid line) and Abramov[2] (green solid line) are also included for comparison. Data are plotted for only half the channel (i.e. above one of the surfaces).

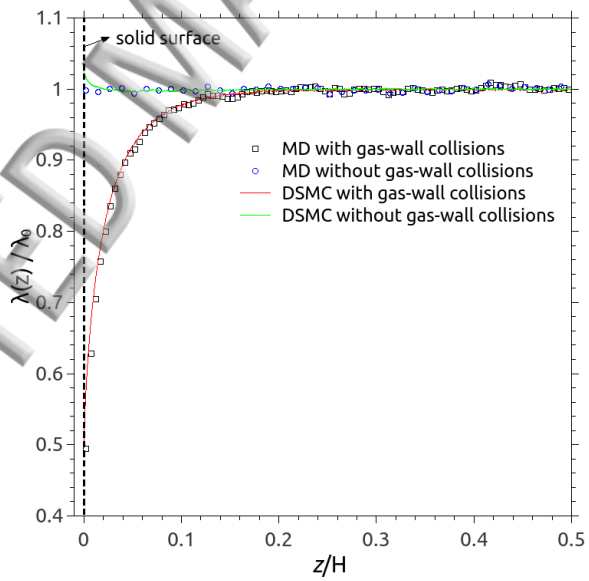

FIG. 5: Spatial variation of the normalised MFP of the gas in a microchannel ($H = 20\lambda_0$). Red and green solid lines refer to the DSMC simulation results that count and do not count the gas-wall collisions, respectively; Open squares (black) and circles (blue) refer to the MD simulation results that count and do not count the gas-wall collisions, respectively. Data are plotted for only half the channel (i.e. above one of the surfaces).

This manuscript was accepted by Phys. Fluids. Click here to see the version of record.

viscosity, such as in Eqs. (1) and (2), is appealing because it allows us to use a modified version of the ubiquitous hydrodynamic Navier-Stokes equations for solving rarefied gas flows, without the large computational expense of DSMC or MD. However, whether this "effective viscosity" is actually effective or is physical, are still unclear. It is also worth stressing that it is not unreasonable that the transport properties of dense fluids in micro/nanochannels differ from those determined in bulk, especially when their are strong inhomogeneities near the confining walls, such as water flows through nanotubes or nanopores [9,15,18,33,45]. The channel heights we are considering in this work are however very large in comparison to the few nanometer dimensions, where such non-continuum transport behaviour are seen to deviate from their bulk description.

In this section we measure viscosity using two independent approaches for three of the lower Knudsen number cases. In the first approach we run Couette simulations and calculate viscosity using the linear stress-strain relationship:

$$\mu(z) = -\frac{\langle P_{xz}(z)\rangle}{\langle \dot{\gamma}(z)\rangle}, \tag{10}$$

where P_{xz} and $\dot{\gamma}$ are the shear stress parallel to the solid wall and the rate of strain, respectively, and the angle brackets denote a time-averaged value from the MD simulations. Note that since the gas is rarefied, no layering occurs at the walls and, therefore, the application of this method is anticipated not to suffer any singularity issues[45]. In Eq. (10), the stress tensor is calculated by using the Irving-Kirkwood approach[21], i.e.

$$\boldsymbol{P} = \frac{1}{V}\left[\sum_i m_i(\boldsymbol{v}_i - \boldsymbol{u})^2 + \frac{1}{2}\sum_{i,j}\boldsymbol{r}_{ij}\boldsymbol{F}_{ij}\right], \tag{11}$$

in which V is the bin volume, $\boldsymbol{v}_i$ is the velocity of the ith gas molecule, $\boldsymbol{r}$ is the relative position between two molecules, $\boldsymbol{u}$ is the local average velocity of the gas flow, and $\boldsymbol{F}$ is the force between two molecules. The first term on the right-hand side of Eq. (11) is the kinetic component, and the second one is the virial component. The kinetic term in the Irving-Kirkwood expression is related to the ideal-gas law, whereas the molecular-molecular virial terms are corrections to the ideal-gas law needed to account for volumes and the force fields between interacting molecules[6].

In the Couette flow problem the gas is sheared by both top and bottom walls, which move with a constant velocity $u_0 = 0.2\sigma_{Ar}/\tau$ in opposite directions along the x axis. This velocity is sufficiently small for thermal effects to be neglected, i.e. the gas flow is isothermal and incompressible. The computational domain is the same as shown in Fig. 2. That is, the distance between the two parallel walls in the z direction is H, and the lengths in both x and y directions are set to λ_0. We select H =

$20\lambda_0$, $10\lambda_0$, $5\lambda_0$, which corresponds to Kn = 0.05, 0.1, 0.2, and, in all these cases, the channel in the z direction is divided into 21 number of bins. The distributions of the strain rate and shear stress across the channel are calculated from the local gradient of the velocity profile and from Eq. (11), respectively. The shear stress and the rate of strain have been averaged over 3×10^6 time steps after the system reached a steady state. A velocity-rescaling thermostat was applied to molecules in the y-direction only, in order to prevent the flow from being perturbed. Figure 6 then shows the local viscosity of the gas across the channel deduced from the linear-response relationship, i.e. Eq. (10). It is apparent that the gas viscosity varies near a solid surface, decreasing with increasing Kn. We observe that the gas viscosity at the wall reduces almost to half the value it has in the bulk (i.e. 49% for Kn = 0.05, 48% for Kn = 0.1, and 44% for Kn = 0.2).

In our second approach we use the Green-Kubo (G-K) equation:

$$\mu = \frac{V}{k_B T}\int_0^\infty \langle P_{xz}(0)P_{xz}(t)\rangle dt, \tag{12}$$

where V is the volume, and the time integration is the ensemble average of the auto-correlation of the stress tensor P_{xz}. The same Kn cases are used as our first method, but now have no moving walls; i.e. there is no flow, and we also divide the system in 7 bins to determine the variation in viscosity. Each case is made larger in the x and y coordinates in order to make the bins contain a large number of molecules for the auto correlation function (ACF), and have a shape which are closer to being cubic. Therefore, for Kn = 0.05, 0.1, 0.2 we changed L_x, L_y to $1.5\lambda_0$, $2\lambda_0$, $3\lambda_0$. Each simulation was run for 40 million time steps, and the ACF is averaged over successive 200k time steps. No thermostat was applied during the measurement of viscosity.

Note, in principle, Eq. (12) only applies to homogeneous systems in the bulk limit but it has been widely used for evaluating the transport coefficients of confined fluids as well[11,19,38]. Here we use the qualitative behaviour of the viscosity from the G-K approach using the largest possible bins we could, as we were not able to produce the same level of resolution as the other two techniques, without running into issues of noise and large computational costs.

We plot in Fig. 6 three independent scaled viscosity calculations: a) the results from our MFP measurements, i.e. Eq. (1), b) the results from the Couette flow, i.e. Eq. (10) and c) the results from Green-Kubo, i.e. Eq. (12). Generally, good agreement is achieved across all three methods.

The viscosity seems to drop by half near the solid wall, and recovers the bulk value for Kn = 0.05 and Kn = 0.1. At Kn = 0.2, viscosity measurements still seem to match up well, but non-equilibrium effects now start to dominate the full channel, rather than confined to the separate

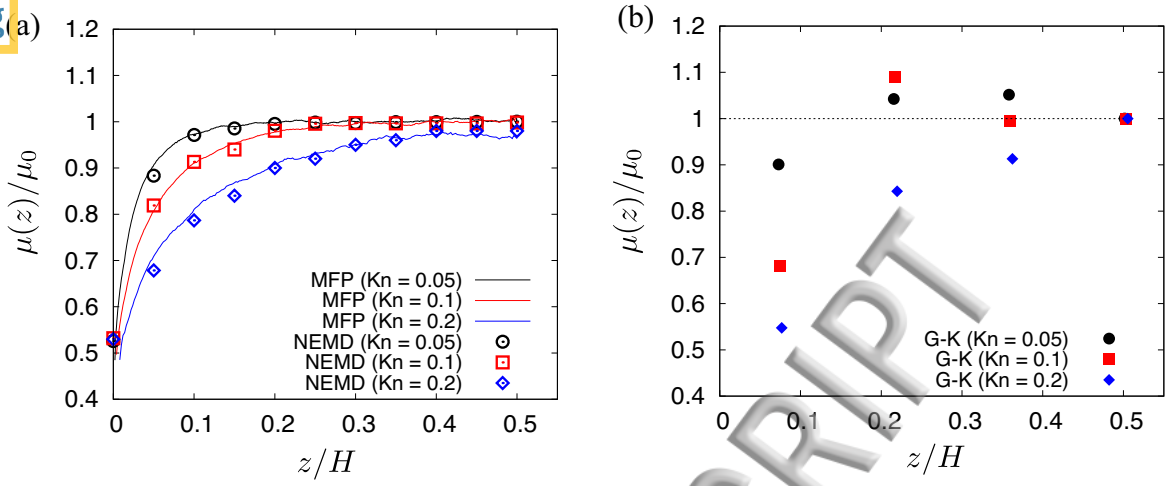

FIG. 6: Local viscosity measurements of gases predicted using (a) the MFP-based scaling law, Eq. (2) and the non-equilibrium MD (NEMD) simulations of Couette flow, Eq. (10), and (b) the Green-Kubo (G-K), Eq. (12), for Kn = 0.05, 0.1, and 0.2. Data are plotted for only half the channel (i.e. above one of the surfaces), and μ_0 is taken to be the bulk viscosity.

Knudsen layers. It is unclear at which stage the definition of viscosity stops being local in rarefied gases. Our work seems to show that it is still relatively accurate to use spatial variations of viscosity up to the early transition Knudsen regime, at least in these simple shear flows.

IV. CONCLUSIONS

The molecular mean free path (MFP) in a confined gas has been numerically evaluated using both the direct simulation Monte Carlo (DSMC) and molecular dynamics (MD) simulations. The MFP has been found to drop smoothly to half of its bulk value near the walls, as long as the collisions between the gas and the wall are accounted for. We demonstrate that the wall-distance dependent MFP is not a numerical artefact but rather a consequence of taking into account the collisions between gas and wall molecules in the calculation of the MFP locally.

In this respect, two main conclusions are made. First, these results are not in disagreement with elementary kinetic theory expressions for the MFP, since these expressions only refer to a spatially homogeneous gas. Second, the answer to the question of whether or not the definition of the MFP should take into account collisions with the solid surfaces depends on the purpose for which the MFP is intended. If it is used to scale transport properties near walls[2,5,17,20,39], then a definition that counts gas-wall collisions should be preferred. This leads to an effective spatially-

varying viscosity derived from the MFP, which agrees well with independent measurements of viscosity using Newton's equation of viscosity from a non-equilibrium Couette flow as well as the Green-Kubo formulation.

The numerical results obtained in the present study have also permitted to assess the theoretical scaling laws for the MFP proposed in the literature so far[2,20]. It turned out that Abramov's scaling law provides the best match with both MD and DSMC results.

A number of future research directions can be envisioned. These include a more detailed analysis of the capability of the MFP-based viscosity to describe gas flows in the early transition regime (including in more complex geometries), as well as the development of a consistent slip boundary conditions to be used within this mathematical framework.

V. ACKNOWLEDGEMENTS

The authors would like to acknowledge the work of Graeme Bird. His influence on the rarefied gas dynamics community has been profound, and through direct and indirect routes inspired the work in this paper, and many others. Finally, the authors would like to dedicate this article to Jason Reese, our co-author, mentor and friend, who passed away in March 2019.

The work is financially supported by the UK's Engineering and Physical Sciences Research Council (EPSRC) via grant nos. EP/N016602/1 and EP/R007438/1. JMR acknowledges the support of the Royal Academy of Engineering under the Chair in Emerging Technologies scheme. JFX thanks the National Natural Science Foundation of China (grant no. 51506110) for their support. OH acknowledges support from the EPSRC Early Career Research Software Engineer Fellowship Scheme (EP/N019180/2). The authors thank Dr Srinivasa Ramisetti for useful discussions.

Appendix A: MD Calibration procedure

In order to directly evaluate the MFP in MD simulations with a continuous interaction potential, a procedure for judging the collision event between two molecules is required, and a collision diameter should be chosen. For argon molecules, Dongari *et al.*[17] and Perumanath Dharmapalan *et al.*[31] suggested $\sigma_{col} = \sigma_{Ar}$, while Barisik and Beskok[7] used $\sigma_{col} = 1.06\sigma_{Ar}$ by combining the basic concept of the MFP for hard spheres given by Eq. (3) and the viscosity-based MFP in Eq. (4).

TABLE II: Comparison of the MFP for a spatially homogeneous gas provided by MD simulations with $\sigma_{col} = \sigma_{Ar}$ and kinetic theory. The values of MFP in brackets are from the ratio of the mean velocity $\bar{u}$ to collision frequency θ, i.e. $\lambda = \bar{u}/\theta$.

	MD			Kinetic theory		
T [K]	$\bar{u}$ [m·s^{-1}]	θ [ns^{-1}]	λ [nm]	$\bar{u}$ [m·s^{-1}]	θ [ns^{-1}]	λ [nm]
273	382.47	5.59	68.55 (68.38)	380.49	6.15	61.89 (61.87)
297	394.62	5.39	73.81 (73.16)	394.18	5.79	68.11 (68.08)
323	414.58	5.14	81.09 (80.59)	413.86	5.33	77.62 (77.65)
373	446.38	4.83	92.56 (92.51)	444.73	4.73	94.12 (94.02)
473	502.65	4.25	118.26 (118.27)	500.79	3.93	127.36 (127.43)

Note that, in fact, λ_h and λ_v differ by a small multiplicative constant: $\lambda_h/\lambda_v = 16/5\pi = 1.02$[28]. To *et al.*[39] adopted $\sigma_{col} = 1.014\sigma_{Ar}$ as a best fit of the predictions of kinetic theory to their calculations of MFP using MD.

To demonstrate the sensitivity of the MFP measurements to the collision diameter, we consider the MFP of argon molecules contained in a cubic domain, with periodic boundary conditions in all directions with the length of each side of the domain set to about one MFP, as given by Eq. (4). We set $\sigma_{col} = \sigma_{Ar}$ and we see in Table II that the subsequent values of MFP from our MD simulations are greater than kinetic theory predictions at low gas temperatures, but smaller at higher gas temperatures. This is not unexpected because molecules have larger kinetic energies at high temperatures and this reduces the collision diameter. The averaged value of the free paths can also be obtained by the ratio of the mean velocity of the gas molecules to the collision frequency between gas molecules, i.e. $\lambda = \bar{u}/\theta$, where the mean velocity is $\bar{u} = \sqrt{8k_BT/\pi m}$, and θ is the collision frequency given by MD. A comparison of the averaged free paths based on the collision frequency and the MFP determined directly from our MD simulations is also made in Table II, and there is a generally good agreement between the two approaches.

In order to recover the kinetic theory prediction of the MFP, i.e. Eq. (4), a temperature-dependent collision diameter is proposed to characterise the collision events between gas molecules. Figure. 7(a) shows a sample simulation result on the variation of MFP with the collision diameter

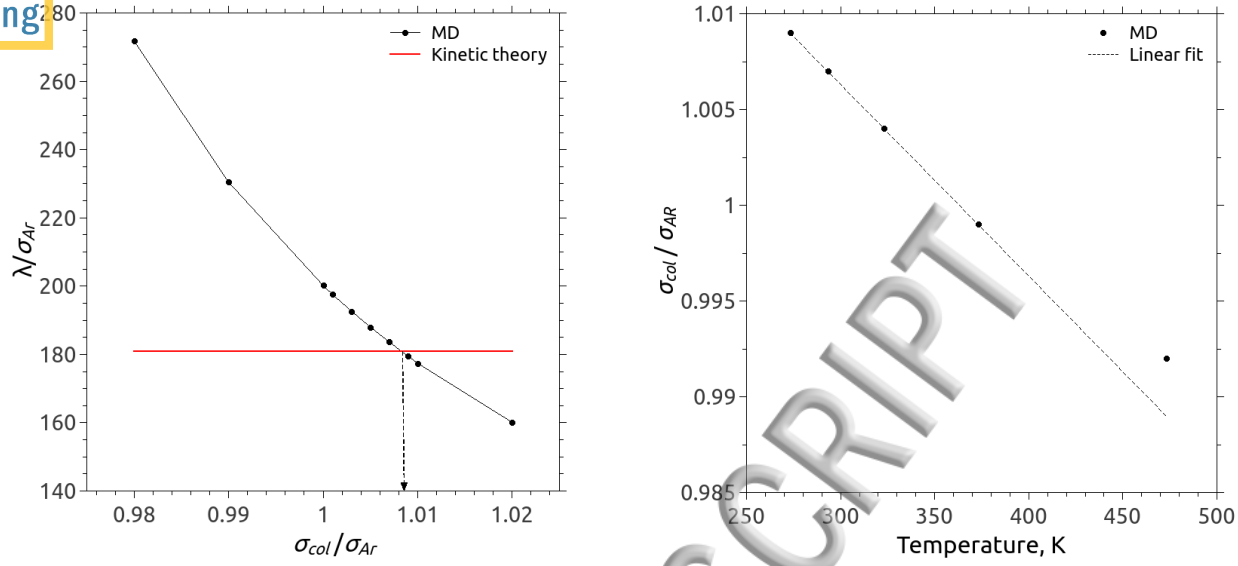

(a) MFP versus the collision diameter at 273 K.

(b) Collision diameter versus temperature.

FIG. 7: Calibration study of the collision diameter σ_{col} for argon in a spatially-homogeneous MD system, where (a) shows the calibration of the collision diameter for a fixed temperature of 273 K that provides the same mean free path as kinetic theory, and (b) shows the final calibrated collision diameters of various temperatures.

at a low gas temperature (i.e. 273 K) for varying prescribed σ_{col} (filled circles). The MD-measured MFP decreases with the increase of the collision diameter, and the intersection with the prediction of kinetic theory, Eq. (4) (red solid line), is when $\sigma_{col} \simeq 1.009\sigma_{Ar}$. Likewise, the approximate collision diameter can be determined over a range of temperatures, and the results are shown by solid black symbols in Fig. 7(b). The collision diameter decreases as the gas temperature increases, and in the range of explored temperatures a linear relationship can be estimated, i.e. $\sigma_{col}(T)/\sigma_{Ar} = 1.0363 - 0.0001T$ with T up to 373 K. As the gas temperature increases ($\sim$ 473 K), the decrease of collision diameter becomes less pronounced and a deviation from the linear fit is observed. Nevertheless, the proposed temperature-dependent collision diameter can guarantee good agreement of the MFP between MD calculations and predictions of kinetic theory for the explored gas temperatures.

Note that, in principle, a temperature-dependent collision diameter can be defined based on the Chapman-Enskog expression of the viscosity for a gas composed of hard spheres[13]:

$$d_h^2 = \frac{5}{16}\frac{1}{\mu}\sqrt{\frac{k_B T}{\pi m}}, \tag{A1}$$

where $\mu(T)$ is the viscosity of LJ fluids[13,30]. However, the collision diameters predicted based on Eq. (A1) differ significantly from the ones provided by MD simulations. Therefore, the calibration procedure described above turns out to be necessary in order to get accurate simulation results.

REFERENCES

[1]Abramov, R. V., "Diffusive boltzmann equation, its fluid dynamics, couette flow and knudsen layers," Physica A **484**, 532–557 (2017).

[2]Abramov, R. V., "Gas near a wall: Shortened mean free path, reduced viscosity, and the manifestation of the knudsen layer in the navier–stokes solution of a shear flow," J. Nonlinear Sci. **28**, 833–845 (2018).

[3]Allen, M. P. and Tildesley, D. J., *Computer Simulation of Liquids* (Clarendon, Oxford, 1987).

[4]Aristov, V., *Direct Methods for Solving the Boltzmann Equation and Study of Nonequilibrium Flows* (Springer, 2001).

[5]Arlemark, E. J., Dadzie, S. K., and Reese, J. M., "An extension to the Navier-Stokes equations to incorporate gas molecular collisions with boundaries," J. Heat Transf. **132**, 041006 (2010).

[6]Barisik, M. and Beskok, A., "Equilibrium molecular dynamics studies on nanoscale-confined fluids," Microfluidics Nanofluid. **11**, 269–282 (2011).

[7]Barisik, M. and Beskok, A., "Molecular free paths in nanoscale gas flows," Microfluidics Nanofluid. **18**, 1365–1371 (2015).

[8]Bird, G. A., *Molecular Gas Dynamics and the Direct Simulation of Gas Flows* (Oxford University Press, Oxford, 1994).

[9]Borg, M. K., Lockerby, D. A., Ritos, K., and Reese, J. M., "Multiscale simulation of water flow through laboratory-scale nanotube membranes," Journal of Membrane Science **567**, 115 – 126 (2018).

[10]Cao, B. Y., Chen, M., and Guo, Z. Y., "Temperature dependence of the tangential momentum accommodation coefficient for gases," Appl. Phys. Lett. **86**, 091905 (2005).

[11]Casanova, S., Borg, M. K., Chew, Y. M. J., and Mattia, D., "Surface-controlled water flow in nanotube membranes," ACS Applied Materials & Interfaces **11**, 1689–1698 (2019).

[12]Cercignani, C., *Slow Rarefied Flows: Theory and Application to Micro-Electro-Mechanical Systems* (Birkhäuser Verlag, Basel - Boston - Berlin).

[13]Chapman, S. and Cowling, T. G., *The mathematical theory of non-uniform gases: an account of*

the kinetic theory of viscosity, thermal conduction and diffusion in gases (Cambridge University Press, Cambridge, 1970).

[14]Darabi, H., Ettehad, A., Javadpour, F., and Sepehrnoori, K., "Gas flow in ultra-tight shale strata," J. Fluid Mech. **710**, 641658 (2012).

[15]Davis, H., "Kinetic theory of flow in strongly inhomogeneous fluids," Chem. Eng. Comm. **58**, 413–430 (1987).

[16]Dimarco, G. and Pareschi, L., "Numerical methods for kinetic equations," Acta Numer. **23**, 369–520 (2014).

[17]Dongari, N., Zhang, Y., and Reese, J. M., "Molecular free path distribution in rarefied gases," J. Phys. D Appl. Phys. **44**, 125502 (2011).

[18]Evans, D. J. and Morriss, G., *Statistical mechanics of nonequilibrium liquids* (Cambridge University Press, 2008).

[19]Giannakopoulos, A., Sofos, F., Karakasidis, T., and Liakopoulos, A., "Unified description of size effects of transport properties of liquids flowing in nanochannels," Int. J. Heat Mass Transf. **55**, 5087–5092 (2012).

[20]Guo, Z. L., Shi, B. C., and Zheng, C. G., "An extended Navier-Stokes formulation for gas flows in the knudsen layer near a wall," Europhys. Lett. **80**, 24001 (2007).

[21]Irving, J. and Kirkwood, J., "The statistical mechanical theory of transport processes. iv. the equations of hydrodynamics," J. Chem. Phys. **18**, 817–829 (1950).

[22]Jiang, S. and Luo, L.-S., "Analysis and accurate numerical solutions of the integral equation derived from the linearized bgkw equation for the steady couette flow," J. Comput. Phys. **316**, 416–434 (2016).

[23]Kennard, E. H., *Kinetic Theory of Gases* (McGraw-Hill Book Company, Inc., New York and London, 1938).

[24]Li, W., Luo, L.-S., and Shen, J., "Accurate solution and approximations of the linearized bgk equation for steady couette flow," Comput. Fluids **111**, 18–32 (2015).

[25]Lilley, C. R. and Sader, J. E., "Velocity gradient singularity and structure of the velocity profile in the knudsen layer according to the boltzmann equation," Phys. Rev. E **76**, 026315 (2007).

[26]Lockerby, D. A., Reese, J. M., and Gallis, M. A., "Capturing the Knudsen layer in continuum-fluid models of nonequilibrium gas flows," AIAA Journal **43**, 1391–1393 (2005).

[27]Lorenzani, S., Gibelli, L., Frezzotti, A., Frangi, A., and Cercignani, C., "Kinetic approach to gas flows in microchannels," Nanosc. Microsc. Therm. **11**, 211–226 (2007).

[28]Morris, D. L., Hannon, L., and Garcia, A. L., "Slip length in a dilute gas," Phys. Rev. A **46**, 5279–5281 (1992).

[29]Muntz, E. P., "Rarefied gas dynamics," Annu. Rev. Fluid Mech. **21**, 387–422 (1989).

[30]Neufeld, P. D., Janzen, A., and Aziz, R., "Empirical equations to calculate 16 of the transport collision integrals $\omega(l,s)^*$ for the Lennard-Jones (12-6) potential," J. Chem. Phys. **57**, 1100–1102 (1972).

[31]P.D., S. H., Prabha, S. K., and Sathian, S. P., "The effect of characteristic length on mean free path for confined gases," Physica A **437**, 68–74 (2015).

[32]Plimpton, S., "Fast parallel algorithms for short-range molecular dynamics," J. Compt. Phys. **117**, 1–19 (1995).

[33]Pozhar, L. A., "Structure and dynamics of nanofluids: Theory and simulations to calculate viscosity," Phys. Rev. E **61**, 1432 (2000).

[34]Rapaport, D. C., *The Art of Molecular Dynamics Simulation* (Cambridge University Press, Cambridge, 1995).

[35]Reese, J. M., Gallis, M. A., and Lockerby, D. A., "New directions in fluid dynamics: non-equilibrium aerodynamic and microsystem flows," Philos. T. Roy. Soc. A **361**, 2967–2988 (2003).

[36]Stops, D. W., "The mean free path of gas molecules in the transition regime," J. Phys. D Appl. Phys. **3**, 685–696 (1970).

[37]Struchtrup, H., *Macroscopic Transport Equations for Rarefied Gas Flows* (Springer, 2005).

[38]Thomas, J. A. and McGaughey, A. J. H., "Reassessing fast water transport through carbon nanotubes," Nano Letters **8**, 2788–2793 (2008).

[39]To, Q. D., Léonard, C., and Lauriat, G., "Free-path distribution and Knudsen-layer modeling for gaseous flows in the transition regime," Phys. Rev. E **91**, 023015 (2015).

[40]Wagner, W., "A convergence proof for bird's direct simulation monte carlo method for the boltzmann equation," J. Stat. Phys. **66**, 1011–1044 (1992).

[41]Wu, L., Ho, M. T., Germanou, L., Gu, X.-J., Liu, C., Xu, K., and Zhang, Y., "On the apparent permeability of porous media in rarefied gas flows," J. Fluid Mech. **822**, 398–417 (2017).

[42]Xie, J.-F. and Cao, B.-Y., "Fast nanofluidics by travelling surface waves," Microfluidics Nanofluid. **21**, 111 (2017).

[43]Xie, J.-F., Sazhin, S. S., and Cao, B.-Y., "Molecular dynamics study of the processes in the vicinity of the n-dodecane vapour/liquid interface," Phys. Fluids **23**, 112104 (2011).

[44]Zhang, J., Fan, J., and Fei, F., "Effects of convection and solid wall on the diffusion in microscale convection flows," Phys. Fluids **22**, 122005 (2010).

[45]Zhang, J., Todd, B., and Travis, K. P., "Viscosity of confined inhomogeneous nonequilibrium fluids," J. Chem. Phys. **121**, 10778–10786 (2004).

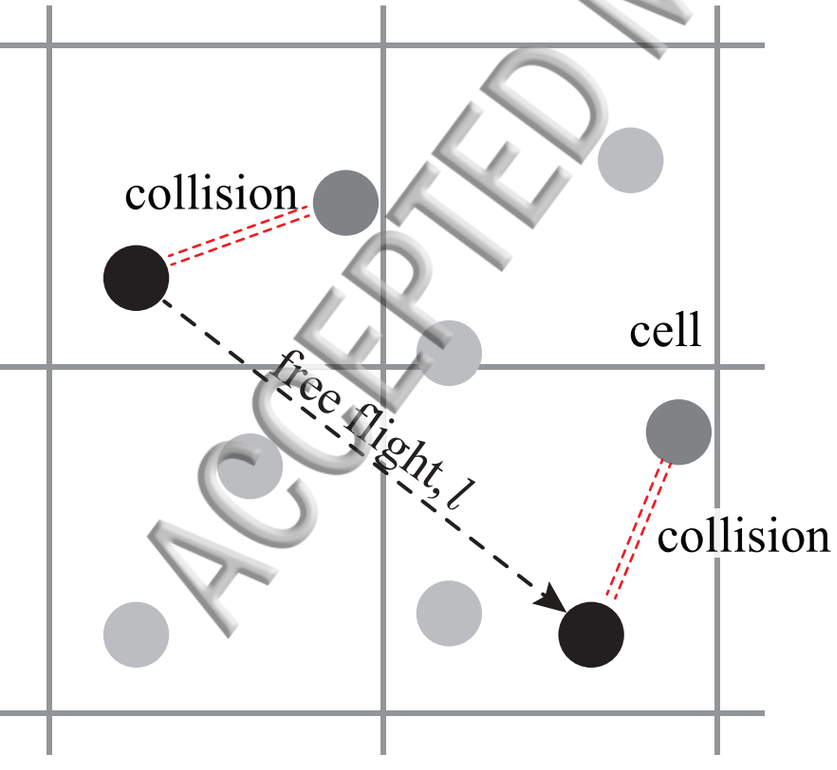

(a) DSMC

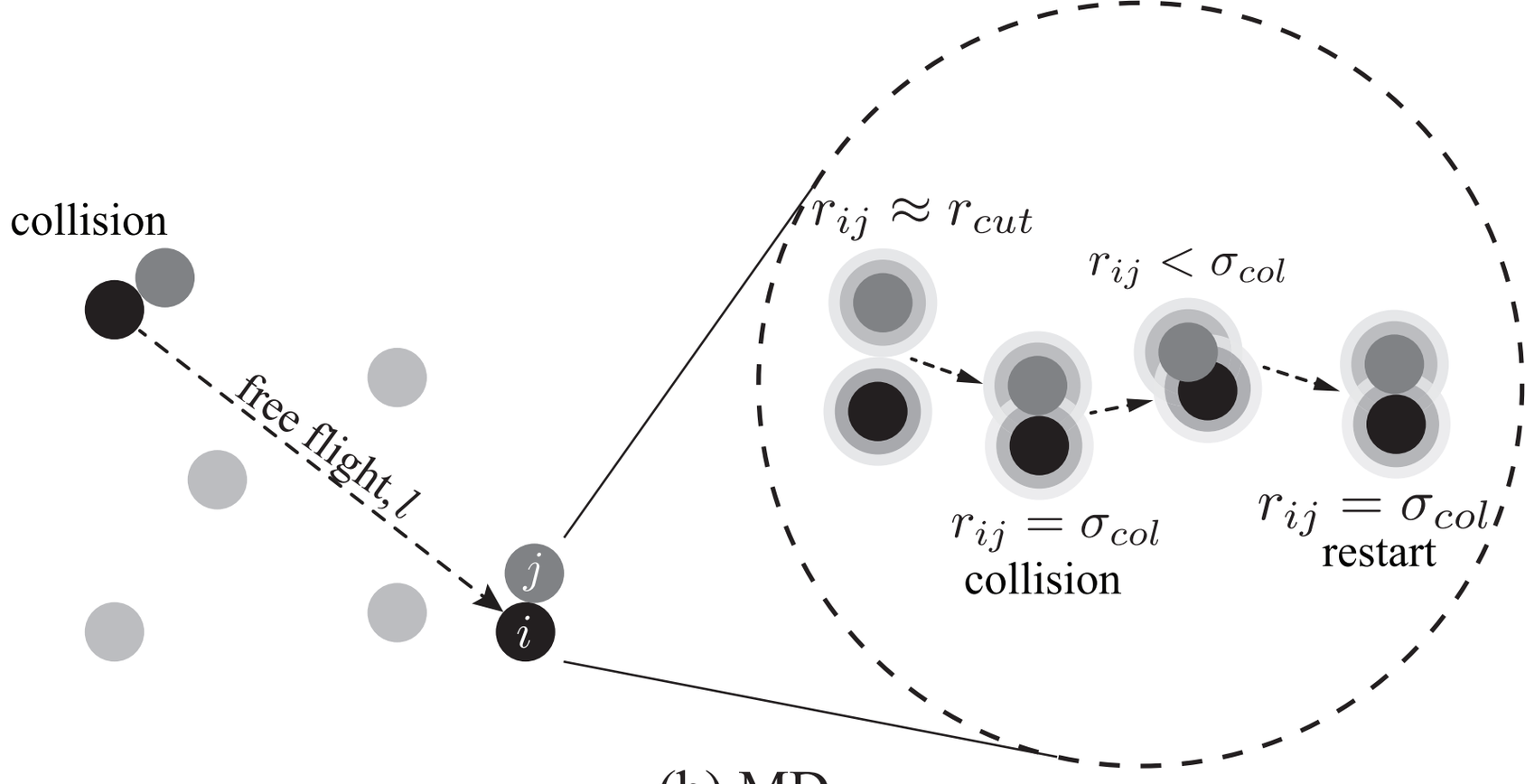

(b) MD

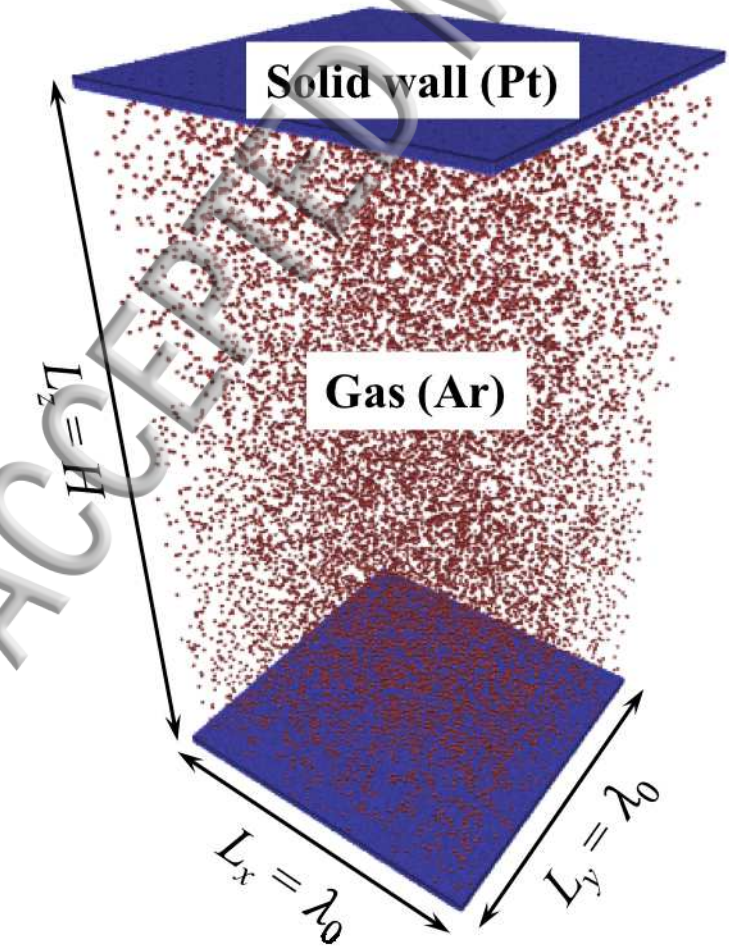

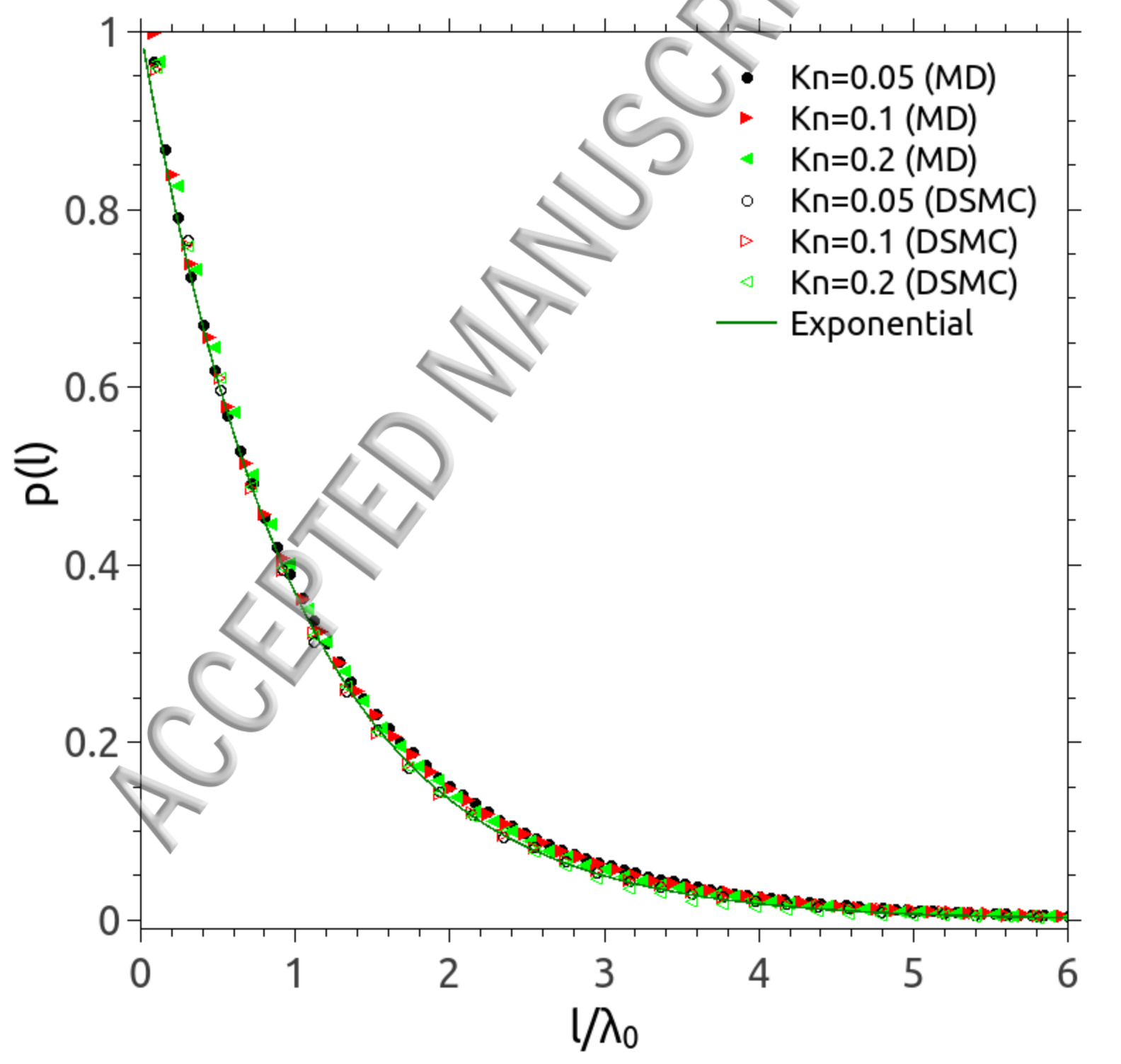

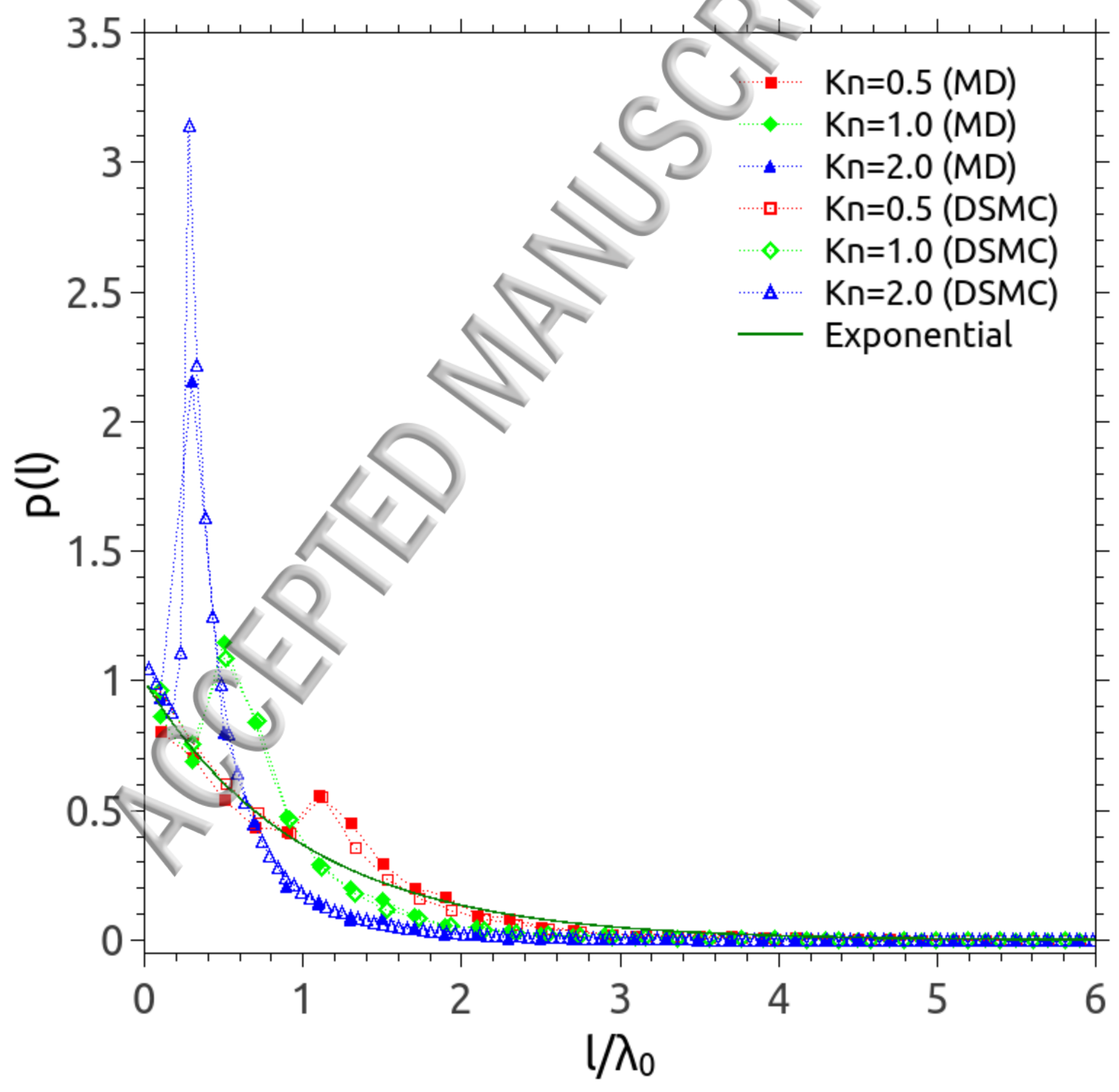

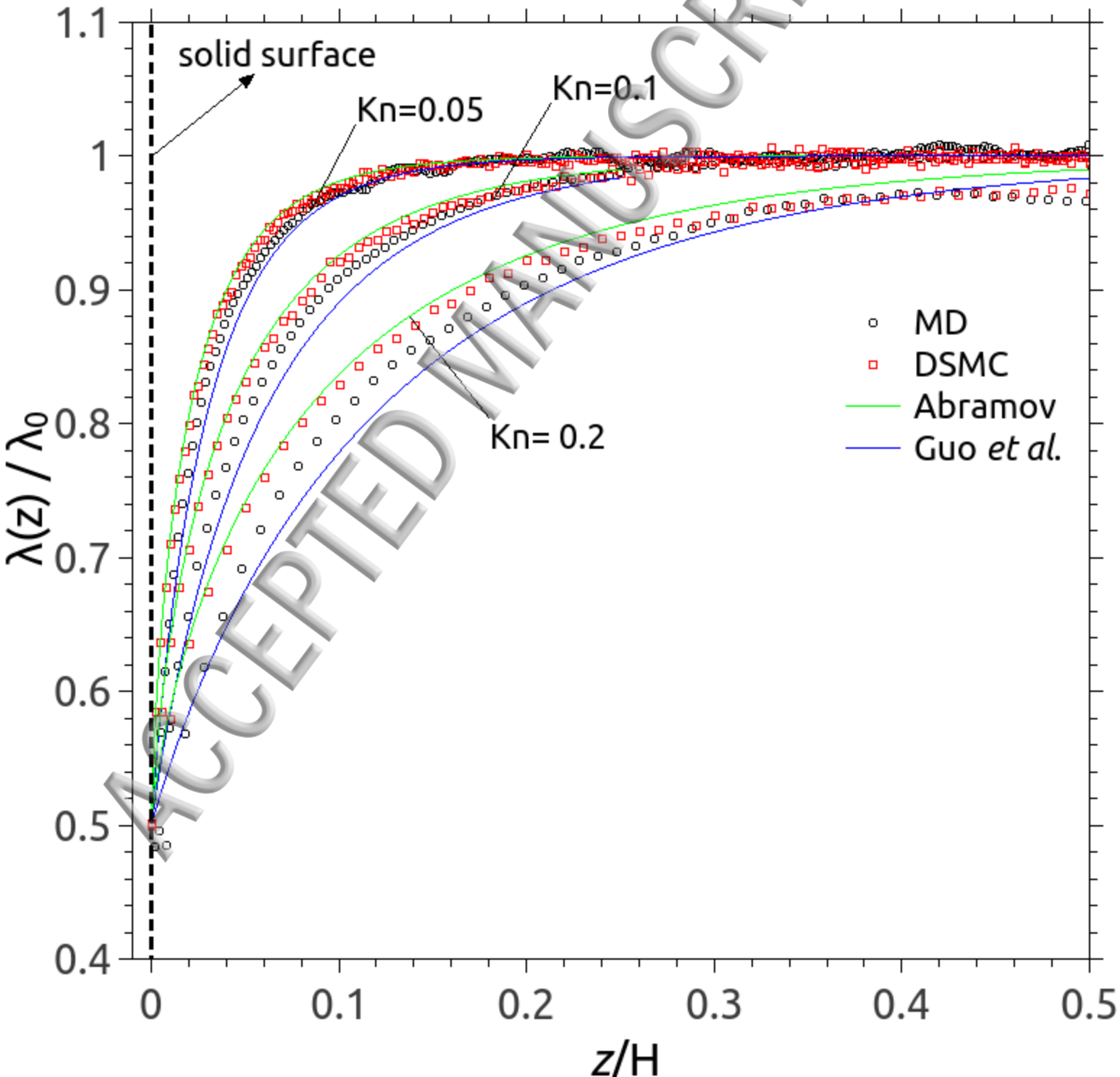

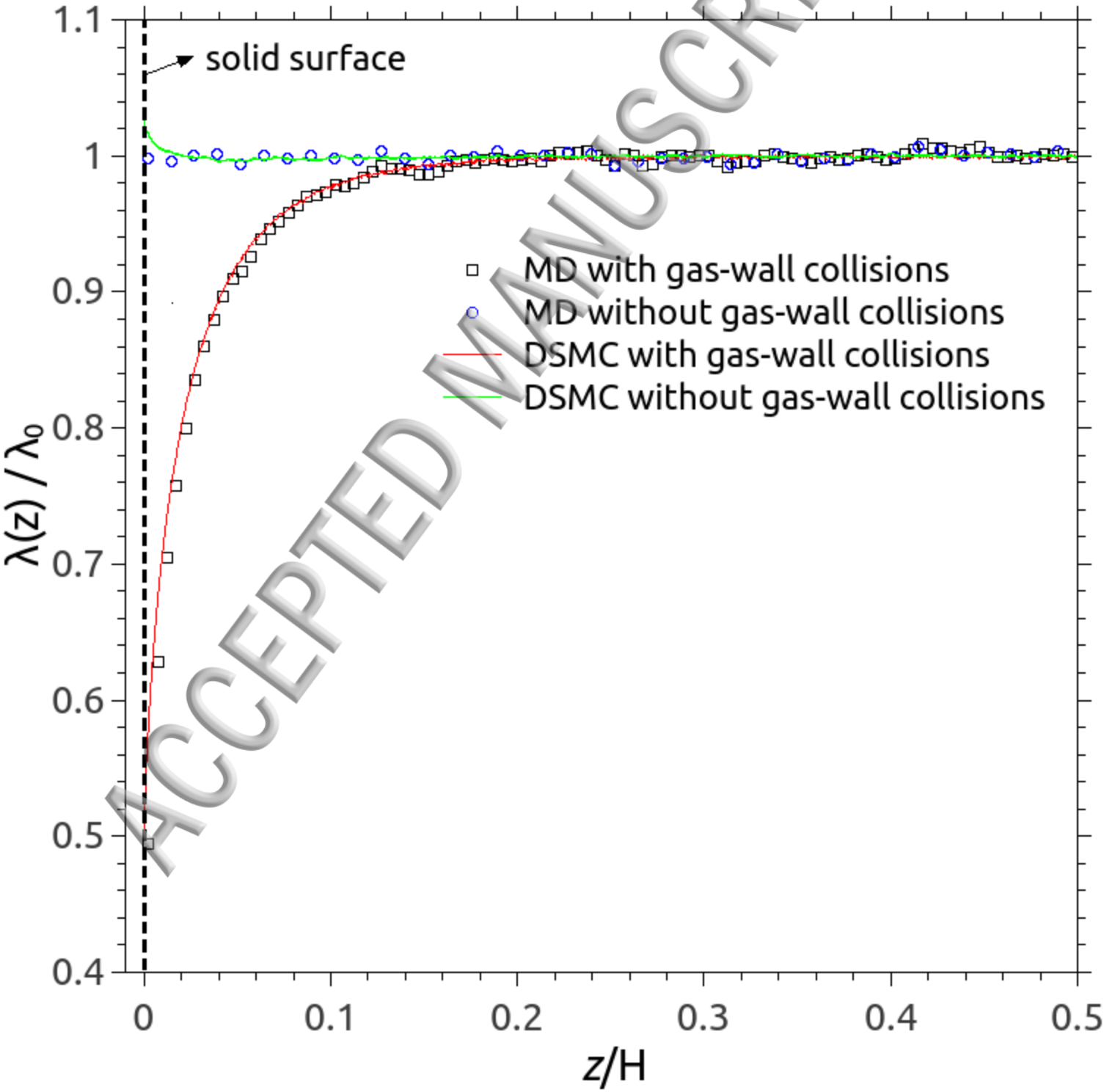

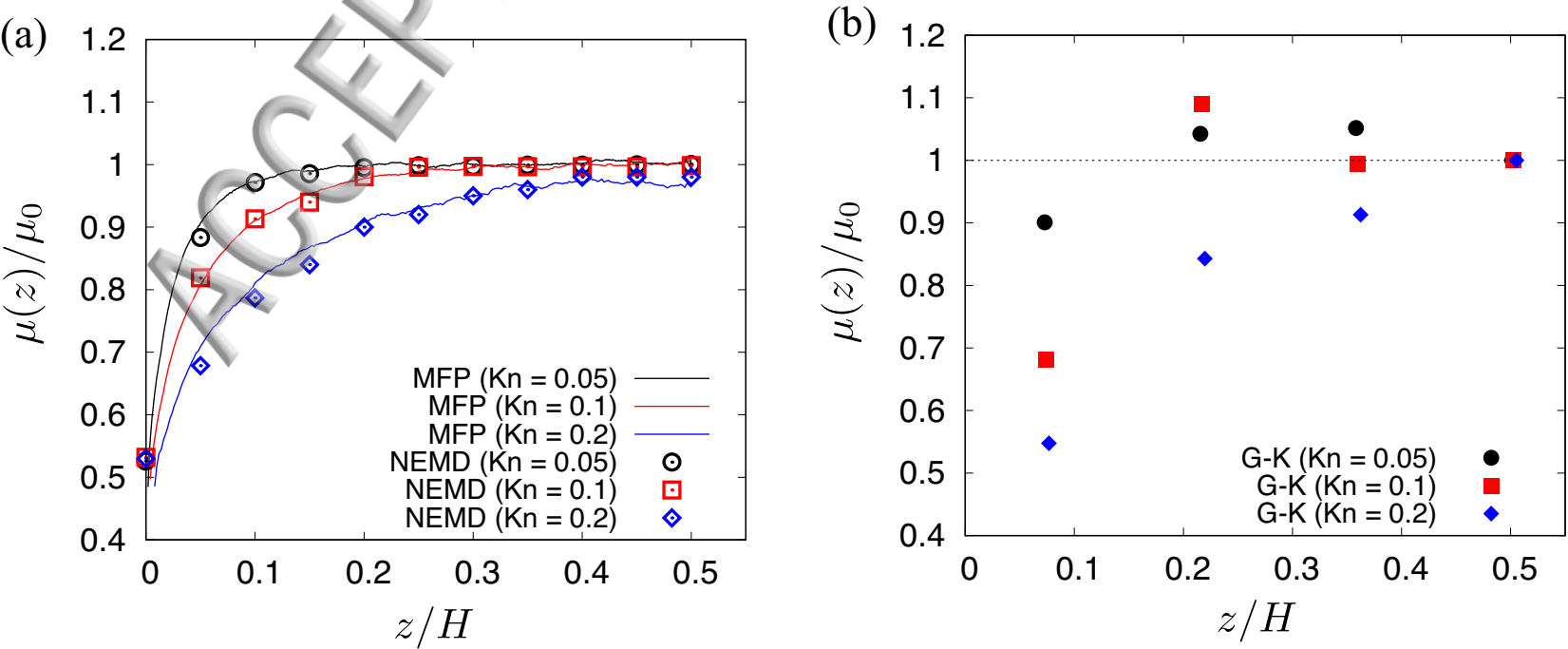
(a)
1.2
1.1
1
0.9
0.8
0.7
0.6
0.5
0.4
$\mu(z)/\mu_0$
0
0.1
0.2
0.3
0.4
0.5
z/H
MFP (Kn = 0.05)
MFP (Kn = 0.1)
MFP (Kn = 0.2)
NEMD (Kn = 0.05)
NEMD (Kn = 0.1)
NEMD (Kn = 0.2)
(b)
1.2
1.1
1
0.9
0.8
0.7
0.6
0.5
0.4
$\mu(z)/\mu_0$
0
0.1
0.2
0.3
0.4
0.5
z/H
G-K (Kn = 0.05)
G-K (Kn = 0.1)
G-K (Kn = 0.2)